

**Electron-induced double ionization of isolated water molecules**D. Oubaziz,<sup>1</sup> C. Champion,<sup>2,\*</sup> and H. Aouchiche<sup>1</sup><sup>1</sup>*Laboratoire de Mécanique, Structures et Energétique, Université Mouloud Mammeri de Tizi-Ouzou, Boîte Postale 17, 15000 Tizi-Ouzou, Algeria*<sup>2</sup>*Centre d'Etudes Nucléaires de Bordeaux Gradignan, Université Bordeaux I, CNRS/IN2P3, Boîte Postale 120, 33175 Gradignan, France*  
(Received 9 July 2013; published 16 October 2013)

Theoretical doubly differential and total cross sections for electron-induced double ionization of oriented water molecules are reported here. The calculations are performed within the first Born approximation by describing the initial molecular state by means of single-center wave functions. Furthermore, the incident (scattered) electron is described by a plane wave while a Coulomb wave function is used for modeling the two secondary ejected electrons. The contribution of each final state to the double-ionization process is analyzed, namely, in considering target electrons ejected either from similar or from different molecular subshells. Thus, secondary electron energetic distributions as well as total cross sections are reported for particular target configurations, pointing out orientation effects in the double-ionization process.

DOI: [10.1103/PhysRevA.88.042709](https://doi.org/10.1103/PhysRevA.88.042709)

PACS number(s): 34.70.+e, 82.30.Fi

**I. INTRODUCTION**

Interactions of charged particles like electrons, positrons, and ions with water molecule are of fundamental importance in many fields including physics [1–4], radiobiology, and even medicine [5,6]. Indeed, the living cells being constituted of about 50–80% water in mass, the water molecule represents an ideal surrogate target to investigate the radio-induced ionizing processes in biological matter. As an example, energy transfer patterns as well as angular distributions resulting from electron-induced collisions with water are commonly used as input data in numerical simulations for modeling the charged-particle track-structure in biological samples (see, for example, Ref. [7] and references therein). In these numerical codes (see, for example, Refs. [8–12] and [13–17] for electron- and ion-track simulations, respectively), the electron histories are described step by step by means of differential and total interaction cross sections in order to provide the most detailed energetic cartography (see, for example, the CELLDOSE code developed by Champion *et al.* [18] devoted to the modeling of the microscopic energetic distribution received by normal tissues or cancer cells in order to assess the relative merits of specific radiopharmaceuticals). Knowledge of the collision dynamics of electrons with biological systems is hence essential over a wide range of energies including the low-energy domain since the observation that high-energy radiations—like those commonly used in cancer treatment planning—liberate many low-energy electrons which may cause additional subcellular damages like DNA single-strand breaks and/or base deletions [19]. In this context, many theoretical models have been proposed in the past for describing the main electron-induced collisional processes in liquid and gaseous water, including ionization, excitation, and even elastic scattering (see Ref. [7] for more details) occulting—most of the time—the double-ionization process considered as minor.

The existing studies on the electron-induced double ionization of molecules remain, up to now, essentially focused on the determination of *multidifferential* cross sections and

therefore limited to simple molecules. In this context, let us cite the works of Chuluunbaatar *et al.* [20] and Mansouri *et al.* [21], both based on the plane-wave Born approximation model (PWBA) and focused on the description of the (*e,3e*) experiments of Lahmam-Bennani *et al.* [22] on a H<sub>2</sub> target. However, in the second work—developed within the second Born approximation [21]—a strong disagreement with the experimental observations [22] was reported by the authors with, in particular, small shifts of the binary and recoil peaks [21]. Let us also cite the more recent experiment of Li *et al.* [23] where double ionization of neon, argon, and molecular nitrogen targets impacted by 600- to 700-eV electron beams was investigated. Thus, the fourfold differential cross sections obtained have demonstrated that the double ionization of small atoms or molecules was dominated—at least within the energy range studied (600–700 eV)—by non-first-order mechanisms such as the two-step (TS2) one, as previously shown by Staicu Casagrande *et al.* [24] for helium. Regarding the double ionization of oriented molecules, there are, to the best of our knowledge, only a few cases reported in the literature. Nevertheless, let us mention the photon- and ion-induced double ionization of molecular deuterium (D<sub>2</sub>) [25] and that of H<sub>2</sub> impacted by photons [26]. For equal energy sharing between the two ejected electrons and the photon ( $\cong 76$  eV), the authors have observed a strong dependence of the electron angular distribution versus the orientation of the molecular target axis. This effect was well reproduced by a model in which a pair of photoionization amplitudes was introduced for the light polarization parallel to as well as perpendicular to the molecular axis. Finally, let us note that orientation effects on ion-induced double ionization have also been recently investigated by Jones *et al.* [27] and Landers *et al.* [28].

From a more “macroscopic” point of view, namely, in considering *total* (integrated) double-ionization cross sections of atoms and molecules, only a few theoretical predictions are available in the literature. Let us cite the pioneer works of Byron and Joachain [29,30] and Tweed [31,32] where *total* double-ionization cross sections by electron impact were estimated as well as the more recent work of Geyer [33] who used a classical trajectory ansatz to describe the double ionization of helium. In this context, quantum-mechanical

\*Corresponding author: [champion@cenbg.in2p3.fr](mailto:champion@cenbg.in2p3.fr)

models remain rarely evoked essentially due to the fact that the latter are usually based on *fully differential* cross-section calculations, which implies numerous successive numerical integrations over the energy and angular transfers in order to access *total* cross sections. This kind of procedure is obviously very time-consuming with regards to computing, which leads to the calculation of total double-ionization cross sections being almost unfeasible, especially at high impact energy. To overcome this limitation, an alternative consists of providing an analytical expression of less differential cross sections. In this context, the partial-wave expansion formalism reported in our previous works appears to be of great interest even if the first achievable cross sections are *sixfold* differential ones, namely, differential in the energy transfers (relative to the two secondary ejected electrons), differential in the scattering direction, differential in the directions of the two ejected electrons, and finally differential in the target molecule orientation, the latter being defined by means of the Euler angle triplets (see hereafter for more details). In this context, let us underline the importance of such *oriented-target* cross sections which appear as crucial not only for a better understanding of the fragmentation mechanism itself but also for practical reasons since anisotropic angular and therefore energetic distributions may influence the measurements, as already revealed by many authors in the case of ion-induced multiple ionization (see, for example, Ref. [34]) as well as in electron-induced ( $e, 2e + M$ ) collisions where the two outgoing electrons and the fragment ion are detected in triple coincidence [35]. Conversely, it has been shown that coincident time-of-flight measurements with a position-sensitive multihit detector provided a complete three-dimensional image of the breakup process for each individual event, conferring then to the measured break-up pattern yields a complete information on the molecular system orientation with respect to the projectile beam axis.

Finally, let us remind the reader that recently, the time-dependent close-coupling (TDCC) method was used to calculate total cross sections for the electron-induced double ionization of helium [36,37], H<sup>-</sup> [38], magnesium [39], and beryllium [40] targets.

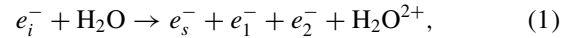
Considering now the investigation of total double-ionization cross sections of oriented molecules, one only finds the case of photon-induced double ionization recently treated by Ivanov and Kheifets [41] who used the time-dependent Schrödinger equation for calculating the *total* double-ionization cross sections of H<sub>2</sub>. Besides, perpendicular to parallel photon-induced double-ionization cross-section ratios were also reported by Vanroose *et al.* [42] and compared to their homologous cross-section ratios obtained by single photoionization. Thus, single-photoionization ratios have shown peaks for photon energy of about 75 eV, which correspond to a Cooper-like minimum of the dipole in the parallel configuration. This maximum was also observed in the photon-induced double-ionization cross-section ratios at slightly lower photon energy. Then, the authors stated that the perpendicular to parallel ratios were similar in both the single- and double-ionization channels.

The double-ionization process on single oriented water molecules is discussed in our previous works [43–45], where *fivefold* differential cross sections for the water double ionization have been reported and intracompared for particular

kinematical conditions in order to highlight the role played by the target molecule orientation in the double-ionization process. In this context, the current work aims to point out that the molecular orientation is still crucial when less differential cross sections are investigated, in particular, in terms of secondary electron energy distribution as well as total cross sections as already observed for the single ionization of oriented water molecules [46].

## II. THEORETICAL MODEL

We here study the double-ionization reaction on water molecule,



where  $e_i^-$ ,  $e_s^-$ ,  $e_1^-$ , and  $e_2^-$  refer to the incident, the scattered, and the two outgoing electrons, respectively, H<sub>2</sub>O<sup>2+</sup> being the residual ion. The corresponding momenta  $\mathbf{k}_i, \mathbf{k}_s, \mathbf{k}_1$ , and  $\mathbf{k}_2$  are linked to the electron kinetic energies via the following relations:  $k_i = \sqrt{2E_i}$ ,  $k_1 = \sqrt{2E_1}$ ,  $k_2 = \sqrt{2E_2}$ , and  $k_s = \sqrt{2(E_i - E_1 - E_2 - I^{2+})}$ , where  $I^{2+}$  denotes the double-ionization threshold and varies according to the two molecular orbitals involved in the collision (see Table I).

In the present work as well as in our previous studies devoted to single and double water ionization by charged particles [43,44,48–51], the frozen-core approximation was used in order to reduce the  $N = 10$ -electron problem to a two-electron system and then to consider only two *active* ejected electrons. In addition, we also assume that the remaining electrons in the doubly charged ion core are unaffected by the ionization process. Consequently, the potential  $V \equiv V(\mathbf{r}_0, \mathbf{r}_1, \mathbf{r}_2)$  involved in the transition matrix element may be written as

$$V(\mathbf{r}_0, \mathbf{r}_1, \mathbf{r}_2) = -\frac{2}{r_0} + \frac{1}{|\mathbf{r}_0 - \mathbf{r}_1|} + \frac{1}{|\mathbf{r}_0 - \mathbf{r}_2|}, \quad (2)$$

TABLE I. Binding energies of the various final states of the double-ionized water molecule. The data are taken from Ref. [47].

Molecular final states	Binding energies (eV)	State multiplicity
$1b_1^{-2}$	39.7	Singlet
$3a_1^{-2}$	44.4	Singlet
$1b_2^{-2}$	52.2	Singlet
$2a_1^{-2}$	83.3	Singlet
$1b_1^{-1}3a_1^{-1}$	41.3	Singlet
	38.6	Triplet
$1b_1^{-1}1b_2^{-1}$	44.9	Singlet
	43.0	Triplet
$1b_1^{-1}2a_1^{-1}$	63.9	Singlet
	57.1	Triplet
$3a_1^{-1}1b_2^{-1}$	47.1	Singlet
	44.9	Triplet
$3a_1^{-1}2a_1^{-1}$	65.2	Singlet
	58.8	Triplet
$1b_2^{-1}2a_1^{-1}$	70.3	Singlet
	63.9	Triplet

where  $\mathbf{r}_0$  denotes the position vector of the incident particle whereas  $\mathbf{r}_i$  is the position vector of the  $i$ th bound electron with respect to the center of the molecule, i.e., the oxygen nucleus.

In the present work as well as in our previous studies devoted to the double ionization of water by charged particles [43,44], the oriented target molecule is described by means of single-center molecular wave functions [52]. The ten bound electrons of the water target molecule are then distributed among five molecular wave functions corresponding to the five molecular orbitals denoted  $1b_1, 3a_1, 1b_2, 2a_1$ , and  $1a_1$ . Each of them is expressed as

$$v_j(\mathbf{r}) = \sum_{k=1}^{N_{at}(j)} a_{jk} \Phi_{n_{jk}l_{jk}m_{jk}}^{\xi_{jk}}(\mathbf{r}), \quad (3)$$

where the radial and angular parts are given by Slater functions and by real solid harmonics, respectively (see Ref. [53] for more details). In Eq. (3),  $N_{at}(j)$  is the number of Slater functions used in the development of the  $j$ th molecular orbital and  $a_{jk}$  is the weight of each real atomic component  $\Phi_{n_{jk}l_{jk}m_{jk}}^{\xi_{jk}}(\mathbf{r})$  (more details can be found in Refs. [48,52], where all the necessary coefficients and quantum numbers are reported).

In the first Born approximation, the *fivefold* differential cross sections  $\sigma^{(5)}(\Omega_1, \Omega_2, \Omega_s, E_1, E_2)$  for the water double

ionization, hereafter denoted 5DCS, are given by

$$\begin{aligned} \frac{d^5\sigma}{d\Omega_1 d\Omega_2 d\Omega_s dE_1 dE_2} &\equiv \sigma^{(5)}(\Omega_1, \Omega_2, \Omega_s, E_1, E_2) \\ &= \sum_{j_1=1}^5 \sum_{j_2 \geq j_1}^5 \sigma_{j_1 j_2}^{(5)}(\Omega_1, \Omega_2, \Omega_s, E_1, E_2) \\ &= (2\pi)^4 \frac{k_1 k_2 k_s}{k_i} \sum_{j_1=1}^5 \sum_{j_2 \geq j_1}^5 |T_{j_1 j_2}|^2, \quad (4) \end{aligned}$$

where  $d\Omega_s, d\Omega_1$ , and  $d\Omega_2$  denote the solid angle directions of the scattered and the two ejected electrons, respectively. The energy intervals of the two ejected electrons are represented by  $dE_1$  and  $dE_2$ .

The transition matrix element denoted as  $T_{j_1 j_2}$  refers to the simultaneous ejection of two electrons from two molecular orbitals labeled  $j_1$  and  $j_2$ , respectively. Moreover, as underlined in our previous works, the above-cited wave functions describing the initial bound states of the water molecule refer to a particular molecular orientation given by the Euler angle triplet  $(\alpha, \beta, \gamma)$ , the latter being defined with respect to the laboratory-fixed frame (see Sec. II for more details).

Under these conditions, the matrix element  $T_{j_1 j_2}$  also depends on the target orientation and may be rewritten as

$$T_{j_1 j_2} \equiv T_{j_1 j_2}(\alpha, \beta, \gamma) = \langle \Psi_f(\mathbf{k}_s, \mathbf{k}_1, \mathbf{k}_2; \mathbf{r}_0, \mathbf{r}_1, \mathbf{r}_2; \alpha_1, \alpha_2) | V(\mathbf{r}_0, \mathbf{r}_1, \mathbf{r}_2) | \Psi_i^{j_1 j_2}(\mathbf{k}_i; \mathbf{r}_0, \mathbf{r}_1, \mathbf{r}_2; \alpha_1, \alpha_2; \alpha, \beta, \gamma) \rangle, \quad (5)$$

where  $\Psi_i^{j_1 j_2}(\mathbf{k}_i; \mathbf{r}_0, \mathbf{r}_1, \mathbf{r}_2; \alpha_1, \alpha_2; \alpha, \beta, \gamma)$  represents the initial state of the system while  $\Psi_f(\mathbf{k}_s, \mathbf{k}_1, \mathbf{k}_2; \mathbf{r}_0, \mathbf{r}_1, \mathbf{r}_2; \alpha_1, \alpha_2)$  stands for the final state.

In Eq. (5), the vectors  $|\alpha_1, \alpha_2\rangle$  indicate the spin of the two active electrons: four possibilities may be identified, namely,  $(u, u)$ ,  $(u, d)$ ,  $(d, u)$ , and  $(d, d)$ , where  $u$  ( $d$ ) refers to a spin up (down). Thus, we have

$$|\alpha_1, \alpha_2\rangle = \left\{ \begin{array}{l} \frac{1}{\sqrt{2}} (|u d\rangle - |d u\rangle) \\ |u u\rangle \\ \frac{1}{\sqrt{2}} (|u d\rangle + |d u\rangle) \\ |d d\rangle \end{array} \right\} \begin{array}{l} \text{for a singlet state,} \\ \\ \text{for a triplet state.} \end{array} \quad (6)$$

Thus, the initial state wave function may be taken as a product of a plane wave  $\varphi(\mathbf{k}_i; \mathbf{r}_0)$  describing the incident electron and the wave function  $\phi_i^{j_1 j_2}(\mathbf{r}_1, \mathbf{r}_2; \alpha, \beta, \gamma)$  referring to the ground state of the water molecule, while the final state is described by the product of two Coulomb wave functions  $[\varphi_c(\mathbf{k}_1; \mathbf{r}_1)$  and  $\varphi_c(\mathbf{k}_2; \mathbf{r}_2)]$  describing the two ejected electrons with a plane wave  $\varphi(\mathbf{k}_s; \mathbf{r}_0)$  for the scattered electron. Thus, we may write

$$\begin{aligned} |\Psi_i^{j_1 j_2}(\mathbf{k}_i; \mathbf{r}_0, \mathbf{r}_1, \mathbf{r}_2; \alpha_1, \alpha_2; \alpha, \beta, \gamma)\rangle &= |\varphi(\mathbf{k}_i; \mathbf{r}_0) \phi_i^{j_1 j_2}(\mathbf{r}_1, \mathbf{r}_2; \alpha, \beta, \gamma)\rangle |\alpha_1, \alpha_2\rangle, \\ \langle \Psi_f(\mathbf{k}_s, \mathbf{k}_1, \mathbf{k}_2; \mathbf{r}_0, \mathbf{r}_1, \mathbf{r}_2; \alpha_1, \alpha_2) | &= \langle \varphi(\mathbf{k}_s; \mathbf{r}_0) \phi_f(\mathbf{k}_1, \mathbf{k}_2; \mathbf{r}_1, \mathbf{r}_2) | \langle \alpha_1, \alpha_2 |. \end{aligned} \quad (7)$$

The functions  $\varphi(\mathbf{k}_i; \mathbf{r}_0)$  and  $\varphi(\mathbf{k}_s; \mathbf{r}_0)$  refer to the plane wave functions associated to the incident and the scattered electron, respectively, while the functions  $\phi_i^{j_1 j_2}(\mathbf{r}_1, \mathbf{r}_2; \alpha, \beta, \gamma)$  and  $\phi_f(\mathbf{k}_1, \mathbf{k}_2; \mathbf{r}_1, \mathbf{r}_2)$  refer to the initial and final wave functions, respectively,

$$\phi_i^{j_1 j_2}(\mathbf{r}_1, \mathbf{r}_2; \alpha, \beta, \gamma) \equiv [\phi_i^{j_1 j_2}(\mathbf{r}_1, \mathbf{r}_2; \alpha, \beta, \gamma)]^\pm = \frac{v_{j_1}(\mathbf{r}_1; \alpha, \beta, \gamma) \times v_{j_2}(\mathbf{r}_2; \alpha, \beta, \gamma) \pm v_{j_1}(\mathbf{r}_2; \alpha, \beta, \gamma) \times v_{j_2}(\mathbf{r}_1; \alpha, \beta, \gamma)}{\sqrt{2}} \quad (8)$$

and

$$\phi_f(\mathbf{k}_1, \mathbf{k}_2; \mathbf{r}_1, \mathbf{r}_2) \equiv [\phi_f(\mathbf{k}_1, \mathbf{k}_2; \mathbf{r}_1, \mathbf{r}_2)]^\pm = \frac{\varphi_c(\mathbf{k}_1; \mathbf{r}_1) \times \varphi_c(\mathbf{k}_2; \mathbf{r}_2) \pm \varphi_c(\mathbf{k}_1; \mathbf{r}_2) \times \varphi_c(\mathbf{k}_2; \mathbf{r}_1)}{\sqrt{2}}. \quad (9)$$

Thus,  $\phi_i^{j_1 j_2}(\mathbf{r}_1, \mathbf{r}_2; \alpha, \beta, \gamma)$  and  $\phi_f(\mathbf{k}_1, \mathbf{k}_2; \mathbf{r}_1, \mathbf{r}_2)$  are symmetric ( $[\phi_i^{j_1 j_2}(\mathbf{r}_1, \mathbf{r}_2; \alpha, \beta, \gamma)]^+$  and  $[\phi_f(\mathbf{k}_1, \mathbf{k}_2; \mathbf{r}_1, \mathbf{r}_2)]^+$ , respectively) when the considered vector  $|\alpha_1, \alpha_2\rangle$  refers to a singlet state and antisymmetric ( $[\phi_i^{j_1 j_2}(\mathbf{r}_1, \mathbf{r}_2; \alpha, \beta, \gamma)]^-$  and  $[\phi_f(\mathbf{k}_1, \mathbf{k}_2; \mathbf{r}_1, \mathbf{r}_2)]^-$ ,

respectively) otherwise. Finally, the functions  $v_j(\mathbf{r}; \alpha, \beta, \gamma)$  reported in Eq. (8) are given by

$$v_j(\mathbf{r}; \alpha, \beta, \gamma) = \sum_{k=1}^{N_{at}(j)} f_{jk}(r) \sum_{\mu=-l_{jk}}^{l_{jk}} D_{\mu, m_{jk}}^{l_{jk}}(\alpha, \beta, \gamma) S_{l_{jk}}^{\mu}(\hat{r}), \quad (10)$$

where  $S_{l_{jk}}^{\mu}(\hat{r})$  and  $D_{\mu, m_{jk}}^{l_{jk}}(\alpha, \beta, \gamma)$  refer to the spherical harmonics in their real form [53] and to the rotation matrix, respectively, the latter being defined by

$$D_{\mu, m_{jk}}^{l_{jk}}(\alpha, \beta, \gamma) = e^{-im_{jk}\alpha} d_{\mu, m_{jk}}^{l_{jk}}(\beta) e^{-i\mu\gamma}, \quad (11)$$

where the quantity  $d_{\mu, m_{jk}}^{l_{jk}}(\beta)$  is given by the Wigner formula

$$d_{\mu, m_{jk}}^{l_{jk}} = \sum_{t=0}^{\tau} (-1)^t \frac{\sqrt{(l_{jk} + \mu)!(l_{jk} - \mu)!(l_{jk} + m_{jk})!(l_{jk} - m_{jk})!}}{(l_{jk} + \mu - t)!(l_{jk} - m_{jk} - t)!t!(t - \mu + m_{jk})!} \xi^{2l_{jk} + \mu - m_{jk} - 2t} \eta^{2t - \mu + m_{jk}}, \quad (12)$$

with  $\xi = \cos(\beta/2)$  and  $\eta = \sin(\beta/2)$ .

Under these conditions and by using the well-known partial-wave expansion of the plane wave as well as that of the Coulomb wave, we get the following expression for the 5DCS [44],

$$\begin{aligned} \frac{d^5\sigma^{\pm}(\alpha, \beta, \gamma)}{d\Omega_1 d\Omega_2 d\Omega_3 dE_1 dE_2} &= (2\pi)^4 \frac{k_1 k_2 k_s}{k_i} g_G(\mathbf{k}_1, \mathbf{k}_2) \sum_{j_1=1}^4 \sum_{j_2 \geq j_1}^4 n \left| \hat{\Pi}_{j_1}(\alpha, \beta, \gamma; \mathbf{k}_1) \left[ \prod_{j_2}(\alpha, \beta, \gamma; \mathbf{k}_2) - \hat{\Pi}_{j_2}(\alpha, \beta, \gamma; \mathbf{k}_2) \right] \right. \\ &\quad \pm \hat{\Pi}_{j_1}(\alpha, \beta, \gamma; \mathbf{k}_2) \left[ \prod_{j_2}(\alpha, \beta, \gamma; \mathbf{k}_1) - \hat{\Pi}_{j_2}(\alpha, \beta, \gamma; \mathbf{k}_1) \right] + \prod_{j_1}(\alpha, \beta, \gamma; \mathbf{k}_1) \hat{\Pi}_{j_2}(\alpha, \beta, \gamma; \mathbf{k}_2) \\ &\quad \left. \pm \prod_{j_1}(\alpha, \beta, \gamma; \mathbf{k}_2) \hat{\Pi}_{j_2}(\alpha, \beta, \gamma; \mathbf{k}_1) \right|^2 \end{aligned} \quad (13)$$

with  $\sigma^-$  and  $n = 3$  for the triplet state and  $\sigma^+$  and  $n = 1$  for the singlet state, where

$$\begin{aligned} \prod_j(\alpha, \beta, \gamma; \mathbf{k}_1) &= \frac{2}{qk_1} \sqrt{\frac{2}{\pi}} \sum_{k=1}^{N_{at}(j)} \sum_{l, m} \sum_{l_1, m_1} X_{jk}^{l, l_1}(k, q) i^{l-l_1} e^{i\sigma_1(\eta_1)} Y_{l_1}^{m_1}(\hat{k}_1) Y_l^{m*}(\hat{q}) \Delta_{l_{jk}, m_1 - m, m_{jk}}(\alpha, \beta, \gamma) (-1)^{m_1} \sqrt{\frac{\hat{l}_1 \hat{l}_{jk}}{4\pi}} \begin{pmatrix} l_1 & l & l_{jk} \\ 0 & 0 & 0 \end{pmatrix} \\ &\quad \times \begin{pmatrix} l_1 & l & l_{jk} \\ -m_1 & m & m_1 - m \end{pmatrix}, \end{aligned} \quad (14)$$

with the momentum transfer defined by  $\mathbf{q} = \mathbf{k}_1 - \mathbf{k}_s$ , and

$$\hat{\Pi}_j(\alpha, \beta, \gamma; \mathbf{k}_1) = \frac{1}{\pi q k_1} \sqrt{\frac{2}{\pi}} \sum_{k=1}^{N_{at}(j)} \sum_{m_1=-l_{jk}}^{l_{jk}} \hat{X}_{jk}^{l_{jk}}(k_1) \Delta_{l_{jk}, m_1, m_{jk}}(\alpha, \beta, \gamma) Y_{l_{jk}}^{m_1}(\hat{k}_1) i^{-l_{jk}} e^{i\sigma_{l_{jk}}(\eta_1)}, \quad (15)$$

where

$$\begin{aligned} \Delta_{l_{jk}, m_{jk}, \mu}(\alpha, \beta, \gamma) &= \frac{D_{\mu, -m_{jk}}^{l_{jk}}(\alpha, \beta, \gamma) - D_{\mu, m_{jk}}^{l_{jk}}(\alpha, \beta, \gamma)}{\sqrt{2}} \quad \text{if } j = 1, \text{ i.e., for the } 1b_1 \text{ orbital,} \\ \Delta_{l_{jk}, m_{jk}, \mu}(\alpha, \beta, \gamma) &= i \frac{D_{\mu, m_{jk}}^{l_{jk}}(\alpha, \beta, \gamma) + D_{\mu, -m_{jk}}^{l_{jk}}(\alpha, \beta, \gamma)}{\sqrt{2}} \quad \text{if } j = 3, \text{ i.e., for the } 1b_2 \text{ orbital,} \\ \Delta_{l_{jk}, m_{jk}, \mu}(\alpha, \beta, \gamma) &= \frac{D_{\mu, m_{jk}}^{l_{jk}}(\alpha, \beta, \gamma) + D_{\mu, -m_{jk}}^{l_{jk}}(\alpha, \beta, \gamma)}{\sqrt{2}} \delta_{m_{jk}, 2} + D_{\mu, m_{jk}}^{l_{jk}}(\alpha, \beta, \gamma) \delta_{m_{jk}, 0} \quad \text{otherwise.} \end{aligned} \quad (16)$$

The radial parts  $X_{jk}^{l, l_1}(k, q)$  and  $\hat{X}_{jk}^{l_{jk}}(k)$  introduced in Eqs. (14) and (15) are expressed as

$$X_{jk}^{l, l_1}(k, q) = \int_0^{\infty} dr r F_{l_1}(k, r) j_l(qr) f_{jk}(r), \quad \hat{X}_{jk}^{l_{jk}}(k) = \int_0^{\infty} dr r F_{l_{jk}}(k, r) f_{jk}(r), \quad (17)$$

where  $F_l(k, r)$  and  $j_l(qr)$  denote the radial hypergeometric function and the Bessel function, respectively, while  $f_{jk}(r)$  refers to the  $jk$ th component of the radial part of the target wave function (for more details we refer the reader to our previous works [48–51]).

Let us note that we have also introduced in Eq. (13) the well-known Gamov factor  $g_G(\mathbf{k}_1, \mathbf{k}_2)$  in order to account for the electron-electron repulsion, namely,

$$g_G(\mathbf{k}_1, \mathbf{k}_2) = \frac{v}{e^v - 1}, \quad \text{with } v = \frac{2\pi}{|\mathbf{k}_1 - \mathbf{k}_2|}. \quad (18)$$

However, when the integrations over the ejection directions  $\hat{k}_1$  and  $\hat{k}_2$  are carried out, we take  $g_G(\mathbf{k}_1, \mathbf{k}_2) = 1$  in order to benefit from the selectivity rules of the complex harmonics. Then, we can write

$$\frac{d^3\sigma^\pm(\alpha, \beta, \gamma)}{d\Omega_s dE_1 dE_2} = \int \int \frac{d^5\sigma^\pm(\alpha, \beta, \gamma)}{d\Omega_1 d\Omega_2 d\Omega_s dE_1 dE_2} d\hat{k}_1 d\hat{k}_2, \quad (19)$$

where  $d\hat{k} = \sin\theta d\theta d\phi$ .

Finally, taking into account the closure relation of the spherical harmonics given by

$$\int \mathbf{Y}_\ell^m(\hat{k}) \mathbf{Y}_{\ell'}^{m'}(\hat{k}) d\hat{k} = \delta_{\ell\ell'} \delta_{mm'}, \quad (20)$$

Eq. (19) may be written as

$$\begin{aligned} \frac{d^3\sigma^\pm(\alpha, \beta, \gamma)}{d\Omega_s dE_1 dE_2} = & \left\{ (2\pi)^4 \frac{k_1 k_2 k_s}{k_i} n \sum_{j_1=1}^4 \sum_{j_2 \geq j_1}^4 [I_{j_1 j_1}(\alpha, \beta, \gamma; k_1) \hat{I}_{j_2}(k_2) + I_{j_2 j_2}(\alpha, \beta, \gamma; k_2) \hat{I}_{j_1}(k_1) + I_{j_1 j_1}(\alpha, \beta, \gamma; k_2) \right. \\ & \times \hat{I}_{j_2}(k_1) + I_{j_2 j_2}(\alpha, \beta, \gamma; k_1) \hat{I}_{j_1}(k_2) + \hat{I}_{j_2}(k_1) \hat{I}_{j_1}(k_2) + \hat{I}_{j_1}(k_1) \hat{I}_{j_2}(k_2) + 2\text{Re}[H_{j_1 j_1}(\alpha, \beta, \gamma; k_1) \\ & \times H_{j_2 j_2}^*(\alpha, \beta, \gamma; k_2)] \pm 2\text{Re}[H_{j_1 j_2}(\alpha, \beta, \gamma; k_1) H_{j_1 j_2}^*(\alpha, \beta, \gamma; k_2)] \pm 2\text{Re}[I_{j_1 j_2}(\alpha, \beta, \gamma; k_1) \hat{I}'_{j_2 j_1}(k_2)] \\ & + \frac{1}{\pi} \{ \mp \text{Re}[\hat{I}'_{j_2 j_2}(k_2) H_{j_1 j_2}(\alpha, \beta, \gamma; k_1)] - \text{Re}[H_{j_1 j_1}(\alpha, \beta, \gamma; k_1) \hat{I}_{j_2}(k_2)] \} \pm 2\text{Re}[\hat{I}'_{j_1}(k_1) I_{j_2 j_1}(\alpha, \beta, \gamma; k_2)] \\ & \pm 2\text{Re}[H_{j_2 j_1}(\alpha, \beta, \gamma; k_2) H_{j_2 j_1}^*(\alpha, \beta, \gamma; k_1)] + \frac{1}{\pi} \{ \mp \text{Re}[\hat{I}'_{j_1 j_2}(k_1) H_{j_2 j_1}(\alpha, \beta, \gamma; k_2)] \\ & - \text{Re}[H_{j_2 j_2}(\alpha, \beta, \gamma; k_2) \hat{I}_{j_1}(k_1)] \} + 2\text{Re}[H_{j_1 j_1}(\alpha, \beta, \gamma; k_2) H_{j_2 j_2}^*(\alpha, \beta, \gamma; k_1)] + \frac{1}{\pi} \{ -\text{Re}[H_{j_1 j_1}(\alpha, \beta, \gamma; k_2) \hat{I}_{j_2}(k_1)] \\ & \mp \text{Re}[H_{j_1 j_2}(\alpha, \beta, \gamma; k_2) \hat{I}'_{j_2 j_1}(k_1)] \} + \frac{1}{\pi} \{ -\text{Re}[\hat{I}_{j_1}(k_2) H_{j_2 j_2}(\alpha, \beta, \gamma; k_1)] \\ & \mp \text{Re}[H_{j_2 j_1}(\alpha, \beta, \gamma; k_1) \hat{I}'_{j_1 j_2}(k_2)] \} \pm \text{Re}[\hat{I}'_{j_2 j_1}(k_1) \hat{I}'_{j_1 j_2}(k_2)] \left. \right\}, \quad (21) \end{aligned}$$

where

$$\begin{aligned} I_{j_1 j_2}(\alpha, \beta, \gamma; k_1) = & \frac{8}{\pi} \frac{1}{q^2 k_1^2} \sum_{k=1}^{N_{at}(j_1)} \sum_{l, m} \sum_{l_1, m_1} X_{j_1 k}^{l, l_1}(k_1, q) i^l Y_l^{m*}(\hat{q}) \Delta_{l_{j_1 k}, m_1 - m, m_{j_1 k}}(\alpha, \beta, \gamma) \sqrt{\frac{\hat{l}_1 \hat{l}_{j_1 k}}{4\pi}} \\ & \times \begin{pmatrix} l_1 & l & l_{j_1 k} \\ 0 & 0 & 0 \end{pmatrix} \begin{pmatrix} l_1 & l & l_{j_1 k} \\ -m_1 & m & m_1 - m \end{pmatrix} \sum_{k'_2}^{N_{at}(j_2)} \sum_{l', m'} X_{j_2 k'_2}^{l', l_1}(k_1, q) i^{-l'} Y_{l'}^{m'}(\hat{q}) \Delta_{l_{j_2 k'_2}, m_1 - m', m_{j_2 k'_2}}(\alpha, \beta, \gamma) \\ & \times \sqrt{\frac{\hat{l}_1 \hat{l}_{j_2 k'_2}}{4\pi}} \begin{pmatrix} l_1 & l' & l_{j_2 k'_2} \\ 0 & 0 & 0 \end{pmatrix} \begin{pmatrix} l_1 & l' & l_{j_2 k'_2} \\ -m_1 & m' & m_1 - m' \end{pmatrix}, \quad (22) \end{aligned}$$

$$\begin{aligned} H_{j_1 j_2}(\alpha, \beta, \gamma; k_1) = & \frac{8}{\pi} \frac{1}{q^2 k_1^2} \sum_{k=1}^{N_{at}(j_1)} \sum_{k'_2}^{N_{at}(j_2)} \sum_{l, m, m_1} X_{j_1 k}^{l, l_{j_2 k'_2}}(k_1, q) i^l Y_l^{m*}(\hat{q}) \hat{X}_{j_2 k'_2}^{l_{j_2 k'_2}}(k_1) \Delta_{l_{j_1 k}, m_1 - m, m_{j_1 k}}(\alpha, \beta, \gamma) \\ & \times \Delta_{l_{j_2 k'_2}, m_1, m_{j_2 k'_2}}^*(\alpha, \beta, \gamma) (-1)^{m_1} \sqrt{\frac{\hat{l}_{j_2 k'_2} \hat{l}_{j_1 k}}{4\pi}} \begin{pmatrix} l_{j_2 k'_2} & l & l_{j_1 k} \\ 0 & 0 & 0 \end{pmatrix} \begin{pmatrix} l_{j_2 k'_2} & l & l_{j_1 k} \\ -m_1 & m & m_1 - m \end{pmatrix}, \quad (23) \end{aligned}$$

$$\hat{I}_j(k_1) = \frac{2}{\pi^3} \frac{1}{q^2 k_1^2} \sum_{k=1}^{N_{at}(j)} [\hat{X}_{j k}^{l_{j k}}(k_1)]^2, \quad (24)$$

and

$$\hat{I}'_{j_1 j_2}(k_1) = \frac{2}{\pi^3} \frac{1}{q^2 k_1^2} \sum_{k=1}^{N_{at}(j_1)} \sum_{k'_2}^{N_{at}(j_2)} \hat{X}_{j_1 k}^{l_{j_1 k}}(k_1) \hat{X}_{j_2 k'_2}^{l_{j_2 k'_2}}(k_1) \delta_{m_{j_1 k}, m_{j_2 k'_2}}. \quad (25)$$

Let us note that the summation over the target initial states does not take into account the inner  $1a_1$  orbital contributions. So, the indexes  $j_1$  and  $j_2$  vary up to 4 [see Eqs. (13) and (21)]. In order to obtain the total (integrated) cross section (TCS), Eq. (21) is numerically integrated over the solid angle  $\Omega_s$  and the ejected energies  $E_1$  and  $E_2$ , namely,

$$\sigma^\pm(\alpha, \beta, \gamma) = \int_0^{E_1 \max} \int_0^{E_2 \max} \int \frac{d^3\sigma^\pm(\alpha, \beta, \gamma)}{d\Omega_s dE_1 dE_2} d\Omega_s dE_1 dE_2. \quad (26)$$

In addition, the scattered electron being, by definition, the most energetic electron in the final state, we have followed the recommendations of DeFrance *et al.* [54] and Bahati *et al.* [55] and defined the upper limits of the integration  $E_{1\max}$  and  $E_{2\max}$  as

$$E_{1\max} = (E_i - I^{2+})/2 \quad \text{and} \quad E_{2\max} = (E_i - I^{2+})/2 - E_1,$$

with

$$E_i = I^{2+} + E_s + E_1 + E_2. \quad (27)$$

### III. RESULTS AND DISCUSSION

In the current work, we investigate the influence of the molecular target orientation on the double-ionization (DI) cross sections. To this end, we have selected particular orientations of the target water molecule, namely, those deduced from the initial target orientation  $(\alpha, \beta, \gamma) = (0, 0, 0)$ —which corresponds to a water molecule situated in the  $yz$  plane with the  $z$  axis parallel to the bisecting line of the molecule—by a  $\beta$  rotation around the  $y$  axis (with  $\beta$  ranging from 0 to  $\pi$ ) in keeping  $\alpha = \gamma = 0$ . These different configurations are hereafter denoted  $R_y(0, \beta, 0)$ . In addition, let us note that, in all the geometries investigated here, the incident momentum  $k_i$  remains collinear to the  $z$  axis (see Fig. 1).

Studying the orientation effect on the DI of an oriented water molecule requires discriminating each molecular subshell contribution. Thus, in Fig. 2, we report the evolution of the total DI cross sections for two target electrons ejected from the same orbital—referred to as  $(1b_1)^{-2}$ ,  $(3a_1)^{-2}$ ,  $(1b_2)^{-2}$ , and  $(2a_1)^{-2}$ —versus the Euler angle  $\beta$  and for different incident energies. In order to compare the evolution of the total cross sections versus the  $\beta$  angle, the latter have been normalized to their  $\beta = 0$  value (i.e., for a parallel orientation).

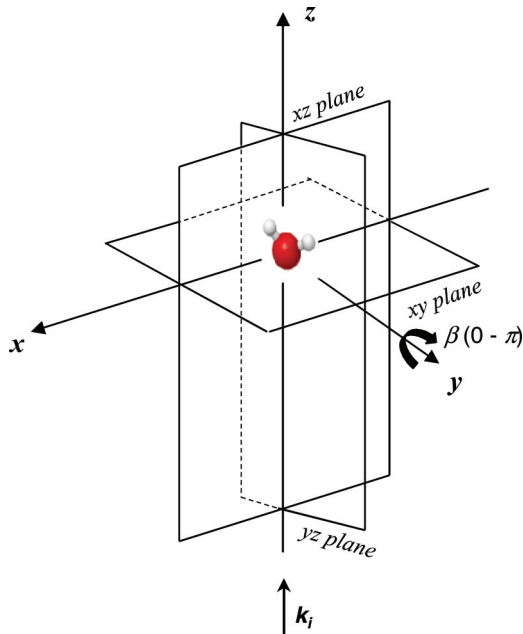


FIG. 1. (Color online) Schematic representation of the particular rotations  $R_y(0, \beta, 0)$  investigated in the present work.

Regarding the  $1b_1$  orbital [see Fig. 2(a)], we note that the total DI cross sections exhibit a maximum at  $\beta = \pi/2$ , whatever the incident energy. This result is consistent with the fact that this orbital is mainly governed by a  $2p_{+1}$  orbital ( $\cong 99.6\%$ ) and then corresponds—in the current molecular description (based on real solid harmonic)—to a molecular orbital collinear to the  $x$  molecular axis. This orbital-type is denoted  $P_X$  in the following. Thus, applying the  $R_y(0, \beta, 0)$  rotation on the  $1b_1$  orbital means going from an initial configuration where the orbital is aligned with the  $x$  axis to a final configuration—denoted  $P_Z$  in the following—where the orbital is parallel to the  $z$  axis, as shown below in Eq. (28), where the  $R_y(0, \beta, 0)$  transformations are summarized:

$$R_y(0, \pi/2, 0) : \begin{cases} P_X \rightarrow P_Z, \\ P_Z \rightarrow P_X, \\ P_Y \rightarrow P_Y. \end{cases} \quad (28)$$

Under these conditions, it clearly appears that the highest DI cross sections are obtained when the impacted orbital is collinear to the beam axis (the  $z$  axis), namely, for  $\beta = \pi/2$ .

Considering now the  $3a_1$  orbital [see Fig. 2(b)]—whose major component is  $2p_0$ , i.e., a  $P_Z$  orbital-type—we observe the opposite trend. Indeed, following the  $R_y(0, \pi/2, 0)$  rotation reported in Eq. (28) according to which a  $P_Z$  orbital becomes a  $P_X$  one, the  $3a_1$  orbital—initially aligned with the incident electron beam—becomes now perpendicular to the incident direction  $(\alpha, \beta, \gamma) = (0, \pi/2, 0)$ , leading then to a minimum for the total DI cross sections at  $\beta = \pi/2$ .

In Fig. 2(c), the total DI cross sections for the  $1b_2$  orbital, mainly governed by a  $2p_{-1}$  orbital, i.e., a  $P_Y$  orbital-type, exhibit a minimum at  $\beta = \pi/2$  while it is clear that the rotation  $R_y(0, \beta, 0)$  should not change the orientation of the molecular orbital, which here remains aligned with the  $y$  axis. This result may be explained by the fact that the  $1b_2$  orbital is not a *pure*  $2p_{-1}$  molecular state since including a non-negligible  $3d_{-1}$  component, which obviously exhibits—in the present real solid-harmonics-based description—four lobes. Under these conditions, this component appears as collinear to the  $P_Z$  orbital for  $(\alpha, \beta, \gamma) = (0, 0, 0)$  while it becomes perpendicular to the incident electron beam after the  $R_y(0, \pi/2, 0)$  rotation. Thus, the total DI cross sections show a minimum for  $\beta = \pi/2$ . Similarly, in Fig. 2(d) the  $s$ -type  $2a_1$  orbital exhibits a maximum for  $(\alpha, \beta, \gamma) = (0, 0, 0)$ , which is due to its non-negligible  $2p_0$  ( $P_Z$ ) component.

Finally, let us note that in all the cases reported in Fig. 2, the DI process seems to be all the more sensitive to the molecule orientation when the incident electron energy is low, as already observed for the single ionization process induced by electron impact on water molecule [46].

Considering now the case of two secondary electrons ejected from two different orbitals, we report in Fig. 3 the relative evolution of the total DI cross sections versus the  $\beta$  angle for different incident energies. The different final states here reported are denoted  $(1b_1)^{-1}(3a_1)^{-1}$ ,  $(1b_1)^{-1}(1b_2)^{-1}$ ,  $(1b_1)^{-1}(2a_1)^{-1}$ ,  $(3a_1)^{-1}(1b_2)^{-1}$ ,  $(3a_1)^{-1}(2a_1)^{-1}$ , and  $(1b_2)^{-1}(2a_1)^{-1}$  in Figs. 2(a)–2(f), respectively.

In Fig. 3(a) we report the case of the  $(1b_1)^{-1}(3a_1)^{-1}$  state, which is mainly governed by a  $(P_X)^{-1}(P_Z)^{-1}$  component. In this case, the incident energy  $E_i = 100$  eV appears as an

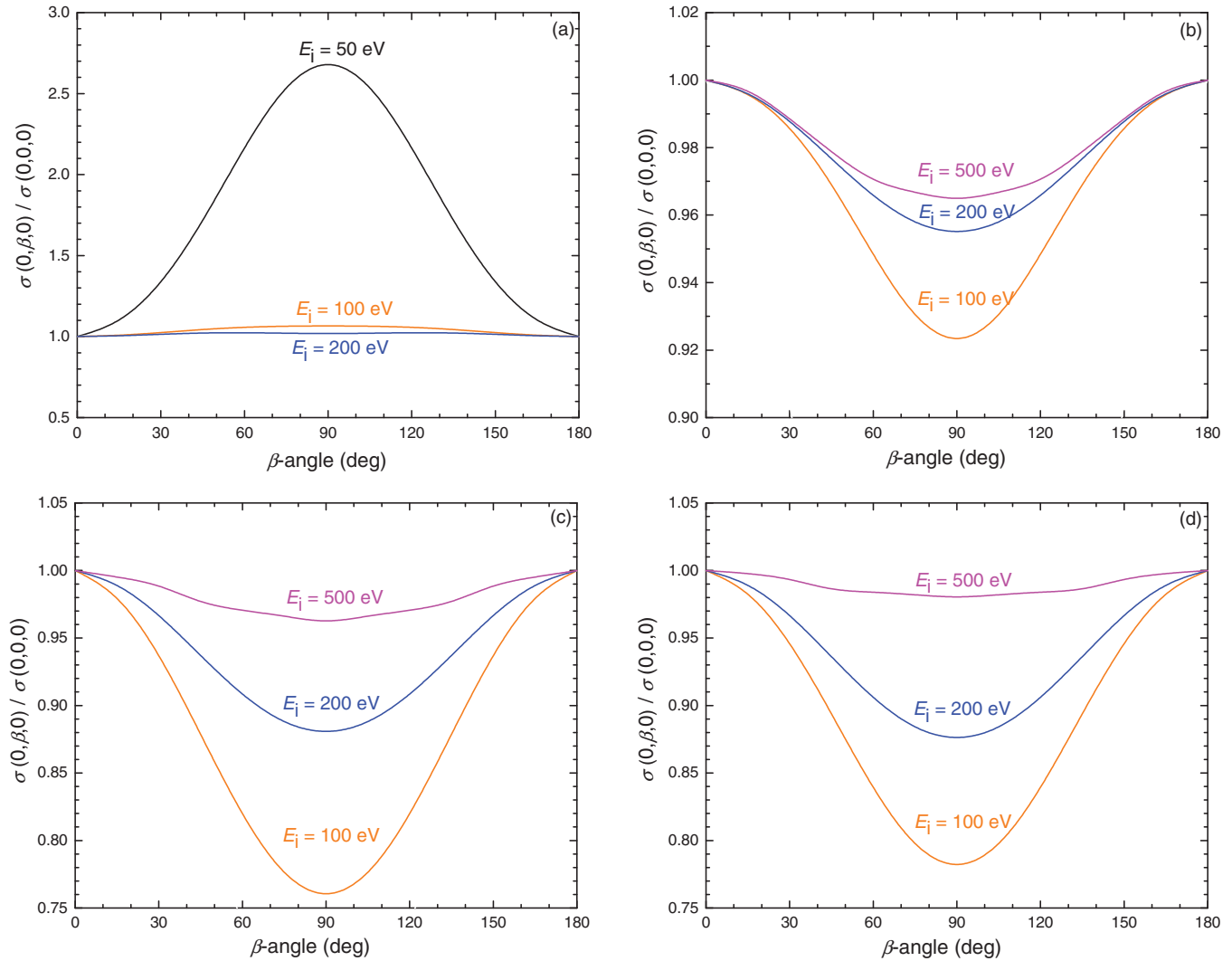


FIG. 2. (Color online) Variation of the total double-ionization cross sections of an isolated water molecule versus the  $\beta$  angle for different incident energies. The secondary electrons considered are here ejected from the same orbital, namely, from (a) the  $1b_1$  orbital, (b) the  $3a_1$  orbital, (c) the  $1b_2$  orbital, and (d) the  $2a_1$  orbital. Curves are normalized at  $\beta = 0$ .

energy threshold. Thus, below this energy “cutoff,” the total DI cross sections appear as essentially influenced by the  $1b_1$  orbital whose behavior is strongly dependent on the  $\beta$  angle for incident energies lower than 100 eV with, in particular, a maximum at  $\beta = \pi/2$  due to its alignment with the incident beam. Thus, the total DI cross sections exhibit a maximum at  $\beta = \pi/2$  for  $E_i < 100$  eV. On the contrary, for  $E_i > 100$  eV, the total DI cross section evolution is essentially due to the  $3a_1$  orbital since the  $1b_1$  orbital shows a quasi-isotropic behavior versus the  $\beta$  angle [see Fig. 2(a)], leading then to a minimum of the total DI cross sections at  $\beta = \pi/2$ .

Similar observations may be done for the  $(1b_1)^{-1}(1b_2)^{-1}$  final state [see Fig. 3(b)] where the behavior of the total DI cross sections is essentially due to the  $1b_1$  component for  $E_i < 100$  eV (with a maximum at  $\beta = \pi/2$ ) whereas the  $1b_2$  component governs the evolution of the total DI cross sections [see Fig. 2(c)] for incident energies greater than 100 eV. However, let us note that the particular case  $E_i = 100$  eV is very interesting since we here observe a minimum at  $\beta = \pi/2$  while

a maximum is reported in Fig. 3(a). This observation may be linked to the value of the ratio  $\sigma(0, \pi/2, 0)/\sigma(0, 0, 0)$ , which is equal to 1.06 for the  $1b_1$  orbital [see Fig. 2(a)], whereas it is equal to 0.76 for the  $1b_2$  orbital [see Fig. 2(c)]. Under these conditions, for this energy,  $E_i = 100$  eV, it is clear that the main contribution to the total DI cross sections is due to the  $1b_2$  orbital which is then responsible for the minimum at  $\beta = \pi/2$ .

The cases reported in, Figs. 3(c), 3(d), and 3(f) show an evident behavior, which may be easily linked to the individual contribution of each molecular orbital involved in the DI process (see Fig. 2). Thus, for all the incident energies considered, we observe a minimum at  $\beta = \pi/2$ . Let us note that the incident energy  $E_i = 50$  eV is not any more considered here since below (or of the same order of magnitude of) the binding energies of the various final states of the double-ionized water molecule (see Table I).

Regarding the  $(3a_1)^{-1}(2a_1)^{-1}$  final state reported in Fig. 3(e), the maximum reported at  $\beta = \pi/2$  for  $E_i = 200$  eV is very interesting since it was not trivially deduced from the

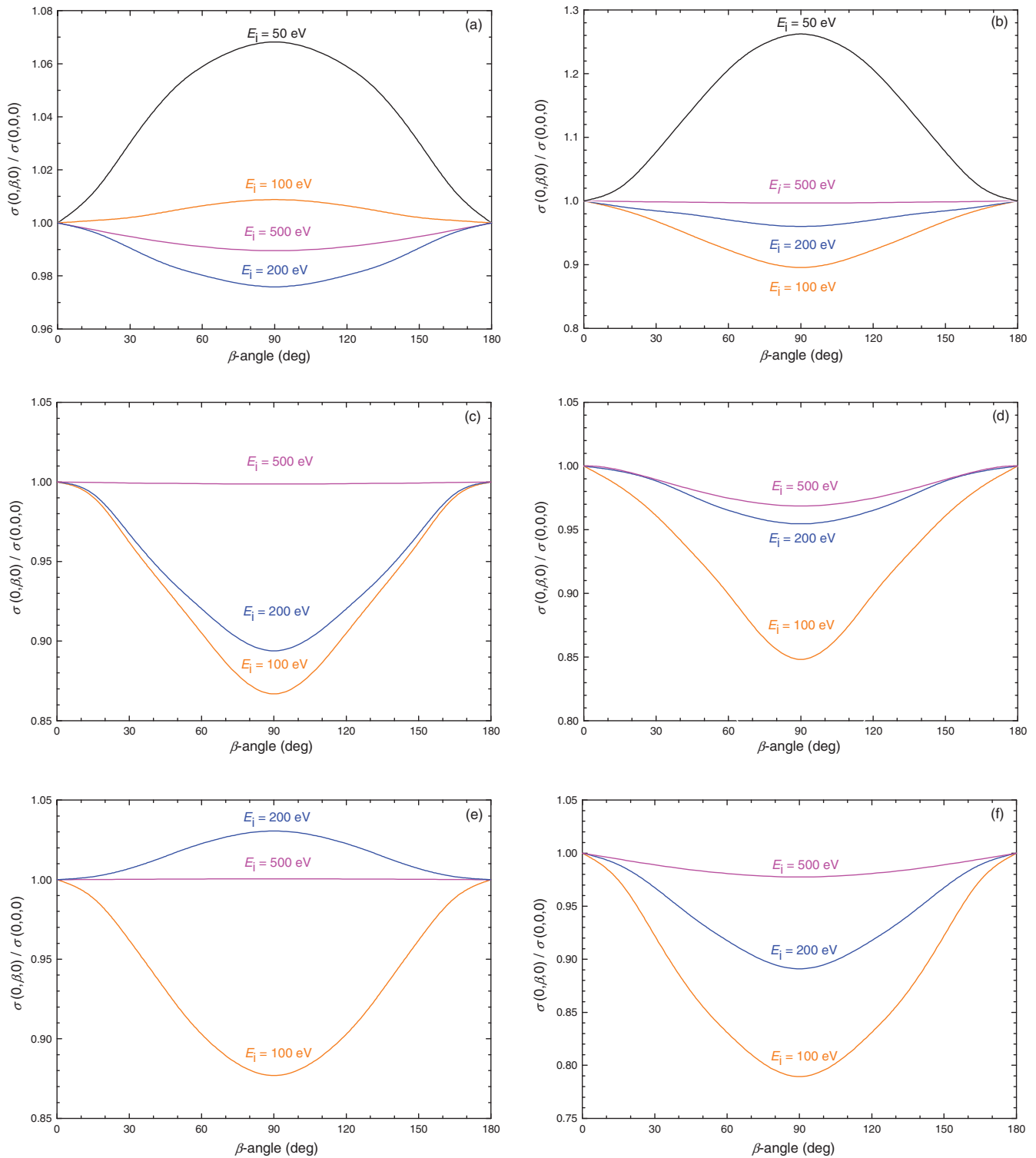


FIG. 3. (Color online) Variation of the total double-ionization cross sections of an isolated water molecule versus the  $\beta$  angle for different incident energies. The secondary electrons considered here are ejected from different orbitals, namely, from (a) the  $(1b_1)^{-1} (3a_1)^{-1}$  state, (b) the  $(1b_1)^{-1} (1b_2)^{-1}$  state, (c) the  $(1b_1)^{-1} (2a_1)^{-1}$  state, (d) the  $(3a_1)^{-1} (1b_2)^{-1}$  state, (e) the  $(3a_1)^{-1} (2a_1)^{-1}$ , and (f) the  $(1b_2)^{-1} (2a_1)^{-1}$  state. Curves are normalized at  $\beta = 0$ .

individual results shown in Fig. 2(b) and Fig. 2(d) for the  $3a_1$  and  $2a_1$  final states, respectively, where a minimum is reported at this  $\beta$  angle. In fact, the observed maximum may be attributed to an *interference effect* between the two considered molecular states, namely, the  $3a_1$  and the  $2a_1$  final states which

both are  $P_Z$  type, contrary to the two particular cases reported in Figs. 3(a) and 3(b) where the molecular states involved in the DI process are orthogonal to each other, namely,  $1b_1$  ( $P_X$ ) and  $3a_1$  ( $P_Z$ ) for Fig. 3(a) and  $1b_1$  ( $P_X$ ) and  $1b_2$  ( $P_Y$ ) for Fig. 3(b). Finally, let us note that we still observe that the DI

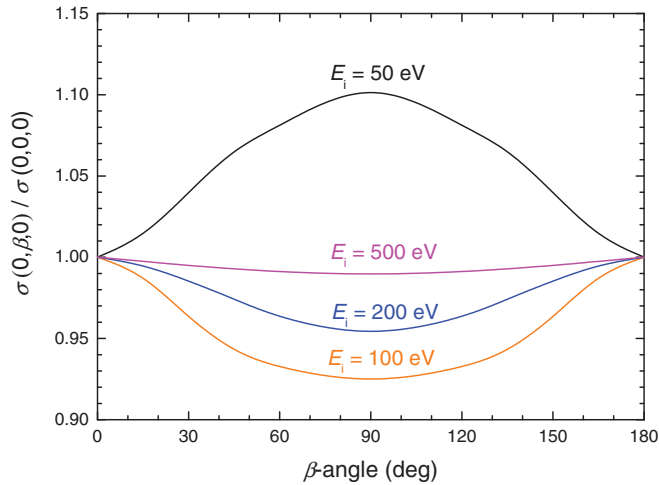


FIG. 4. (Color online) Variation of the *global* double-ionization cross sections of water molecules versus the  $\beta$  angle for different incident energies. Curves are normalized at  $\beta = 0$ .

process is less and less sensitive to the molecule orientation when the incident electron energy increases.

In Fig. 4, we report the evolution of the *global* double ionization cross sections versus the  $\beta$  angle, the latter being obtained by summing up all the molecular-state contributions.

For  $E_i = 50$  eV, we observe that the DI probability shows a maximum for the orientation  $(\alpha, \beta, \gamma) = (0, \pi/2, 0)$  while the parallel orientation  $(\alpha, \beta, \gamma) = (0, 0, 0)$  becomes the preponderant one when the incident energy increases ( $E_i > 50$  eV). This result is undoubtedly attributed to the fact that for  $E_i = 50$  eV, the DI process essentially involves the  $(1b_1)^{-2}$ ,  $(1b_1)^{-1}(3a_1)^{-1}$ , and  $(1b_1)^{-1}(1b_2)^{-1}$  final states for which the DI was privileged in the perpendicular molecular target orientation [see Figs. 2(a), 3(a), and 3(b)]. Then, when the incident energy increases, all the molecular states contribute to the DI process, leading to a maximal cross section for the  $(\alpha, \beta, \gamma) = (0, 0, 0)$  orientation. This feature may be also pointed out when the kinetic energy distributions of the ejected electrons are considered.

Indeed, from Fig. 5 where the global energy distributions of the secondary electrons ejected by double ionization of a water molecule oriented in the  $(0, 0, 0)$  and  $(0, \pi/2, 0)$  directions are shown, it clearly appears that, for the 100-eV electron impact, the DDCS are more affected by the target orientation than for the 500-eV electron impact. Thus, in Figs. 5(a) and 5(b), we observe more pronounced energy distributions with a maximum of about 18 a.u. in the  $(0, 0, 0)$  direction versus about 16 a.u. in the  $(0, \pi/2, 0)$  direction. On the contrary, when the incident electron energy increases, this anisotropy is less evident such as reported in Figs. 5(c) and 5(d) where the

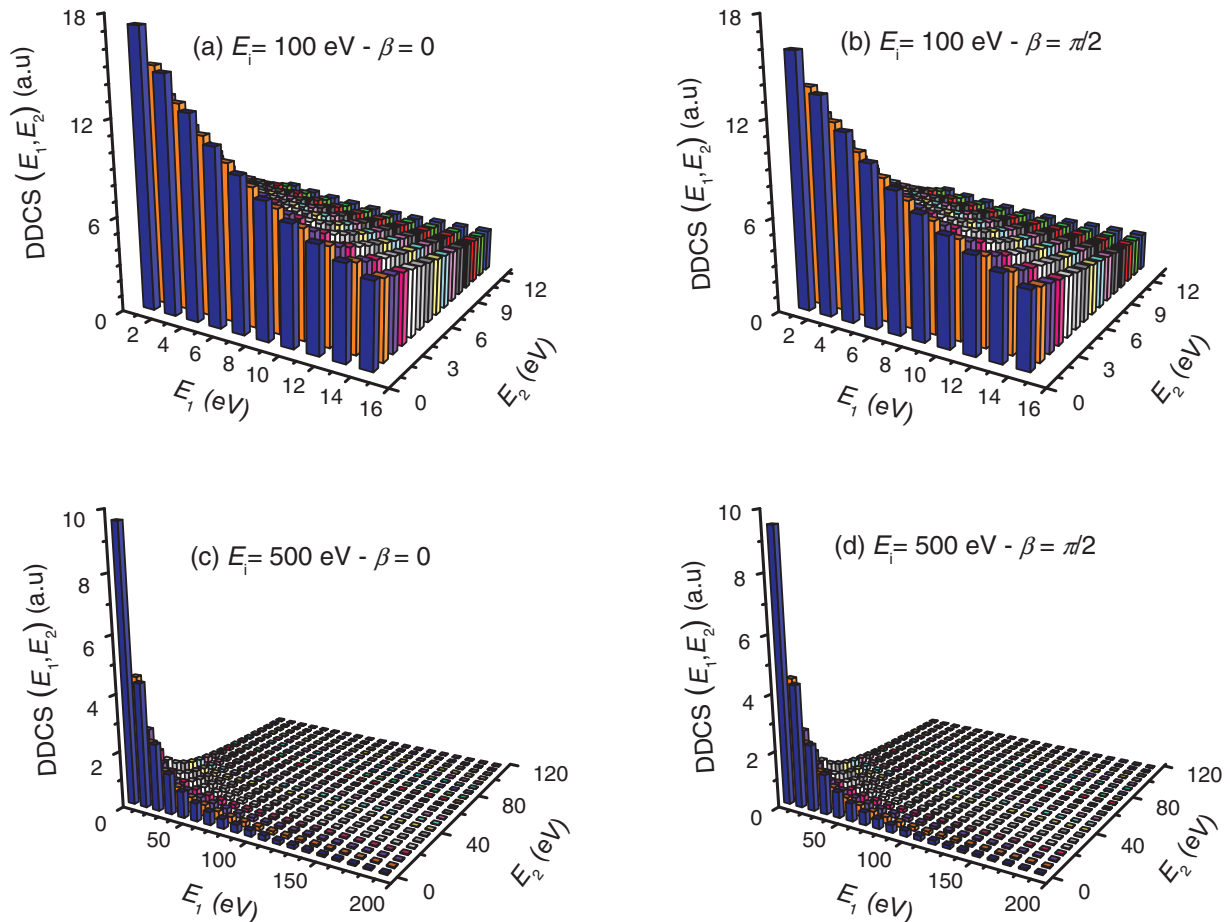


FIG. 5. (Color online) Energetic distributions for the double ionization of an oriented water molecule: (a)  $(E_i, \beta) = (100 \text{ eV}, 0)$ , (b)  $(E_i, \beta) = (100 \text{ eV}, \pi/2)$ , (c)  $(E_i, \beta) = (500 \text{ eV}, 0)$ , and (d)  $(E_i, \beta) = (500 \text{ eV}, \pi/2)$ .

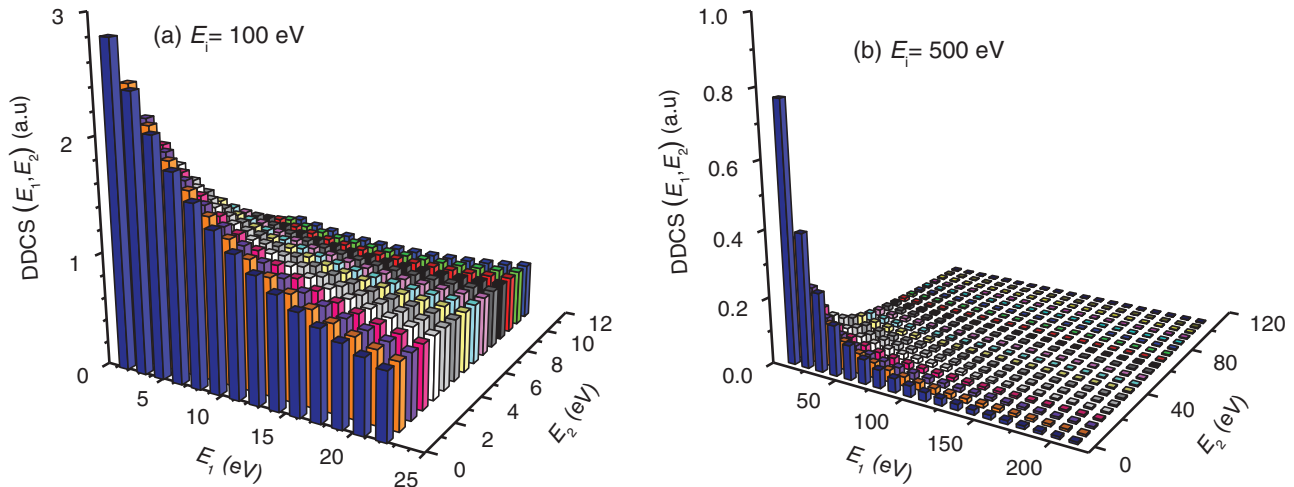


FIG. 6. (Color online) Energetic distributions for the double ionization of a water molecule randomly oriented in the space: (a)  $E_i = 100$  eV and (b)  $E_i = 500$  eV.

energy distribution after a 500-eV electron-induced double ionization is reported for both a  $(0,0,0)$  direction and a  $(0,\pi/2,0)$  direction, respectively.

Finally, we have calculated the *average* energy distributions, analytically deduced from the previous ones by integration over the Euler solid angle. They are reported in Fig. 6 for the two incident energies here investigated, namely,  $E_i = 100$  eV and  $E_i = 500$  eV. We clearly observe a behavior similar to that previously, with nevertheless an evident decrease in terms of magnitude for the doubly differential cross sections, which strongly points out the importance of the *oriented-target* studies, in particular, to appraise at best the underlying physics of the mechanisms involved in the electron-induced molecular fragmentation.

#### IV. CONCLUSION

We have investigated the target orientation dependence of the total double ionization cross sections as well as the secondary energy distributions by using a first Born approximation based model in which the water target molecule was described by means of an accurate single-center molecular target wave function. For each molecular state, the observations reported here—in terms of preferential orientations for DI induction—were qualitatively explained. From a general point of view, it has been clearly reported that the DI process was sensitive to the molecule orientation all the more the incident electron energy is low, the total DI cross sections showing

even an evident anisotropy for incident energies greater than about 500 eV. Moreover, thanks to an acute analysis of the individual contributions of each final state, the dependence of the total DI cross sections versus the target molecular plane orientation has been studied in detail. Thus, for two secondary electrons extracted from the same orbital, it has been shown that the maximal (minimal) cross sections were obtained when the impacted orbital was aligned (perpendicular) with the electron beam. On the other hand, when different orbitals have been involved in the DI process, it has been reported that the individual behavior of the dominant molecular orbital might explain the observation, in pointing out an evident interference effect when the two molecular orbitals considered are of identical type.

Considering now the secondary electron energy distributions, we have also demonstrated that the latter were affected by the target orientation provided that the incident electron energy remains low, namely, lower than 100 eV, with an evident anisotropic shape for higher energies. Besides, we have also showed that the consideration of the target orientation for describing the DI process is all the more important because modeling this kind of complex interaction by means of average cross sections clearly underestimates the magnitude of the double-ionizing process and undoubtedly hides the fine mechanisms involved in the electron-induced molecular fragmentation. Finally, note that at this stage no direct comparison with experiment is possible and we hope that these current predictions will be in the near future confirmed by experimental observations.

- [1] E. W. McDaniel, J. B. A. Mitchell, and M. E. Rudd, *Atomic Collision* (Wiley, New York, 1993).  
 [2] C. S. Enos, A. R. Lee, and A. G. Brenton, *Int. J. Mass Spectrom. Ion Processes* **104**, 137 (1991).  
 [3] K. Mitsuke, T. Takami, and K. Ohno, *J. Chem. Phys.* **91**, 1618 (1989).

- [4] D. H. Katayama, R. E. Huffman, and C. L. O'Bryan, *J. Chem. Phys.* **59**, 4309 (1973).  
 [5] G. H. Olivera, C. Caraby, P. Jardin, A. Cassimi, L. Adoui, and B. Gervais, *Phys. Med. Biol.* **43**, 2347 (1998).  
 [6] M. Dingfelder, M. Inokuti, and H. G. Paretzke, *Radiat. Phys. Chem.* **59**, 255 (2000).

- [7] C. Champion, *Phys. Med. Biol.* **48**, 2147 (2003).
- [8] S. Uehara, H. Nikjoo, and D. T. Goodhead, *Phys. Med. Biol.* **38**, 1841 (1993).
- [9] H. G. Paretzke, in *Kinetics of Nonhomogeneous Processes*, edited by G. R. Freeman (Wiley, New York, 1987), p. 89.
- [10] V. A. Semenenko, J. E. Turner, and T. B. Borak, *Radiat. Environ. Biophys.* **42**, 213 (2003).
- [11] I. Plante and F. A. Cucinotta, *New J. Phys.* **11**, 063047 (2009).
- [12] F. A. Cucinotta, H. Nikjoo, and D. T. Goodhead, *Radiat. Res.* **153**, 459 (2000).
- [13] A. Chatterjee and W. R. Holley, *Adv. Radiat. Biol.* **17**, 181 (1993).
- [14] J. Medin and P. Andreo, *Phys. Med. Biol.* **42**, 89 (1997).
- [15] S. Uehara, L. H. Toburen, and H. Nikjoo, *Int. J. Radiat. Biol.* **77**, 139 (2001).
- [16] S. Uehara and H. Nikjoo, *J. Phys. Chem. B* **106**, 11051 (2002).
- [17] C. Champion, A. L'Hoir, M.-F. Politis, P. D. Fainstein, R. D. Rivarola, and A. Chetoui, *Radiat. Res.* **163**, 222 (2005).
- [18] C. Champion, P. Zanotti-Fregonara, and E. Hindié, *J. Nucl. Med.* **49**, 151 (2008).
- [19] B. Boudaiffa, P. Cloutier, D. Hunting, M. A. Huels, and L. Sanche, *Science* **287**, 1658 (2000).
- [20] O. Chuluunbaatar, B. Joulakian, I. V. Puzynin, K. H. Tsookhuu, and S. I. Vinitzky, *J. Phys. B* **41**, 015204 (2008).
- [21] A. Mansouri, C. Dal Cappello, S. Houamer, I. Charpentier, and A. Lahmam-Bennani, *J. Phys. B* **37**, 1203 (2004).
- [22] A. Lahmam-Bennani, A. Duguet, and S. Roussin, *J. Phys. B* **35**, L59 (2002).
- [23] C. Li, A. Lahmam-Bennani, E. M. Staicu Casagrande, and C. Dal Cappello, *J. Phys. B: At. Mol. Opt. Phys.* **44**, 115201 (2011).
- [24] E. M. Staicu Casagrande, C. Li, A. Lahmam-Bennani, C. Dal Cappello, M. Schulz, and M. Ciappina, *J. Phys. B: At. Mol. Opt. Phys.* **44**, 055201 (2011).
- [25] Th. Weber, A. Czasch, O. Jagutzki, A. Müller, V. Mergel, A. Kheifets, J. Feagin, E. Rotenberg, G. Meigs, M. H. Prior, S. Daveau, A. L. Landers, C. L. Cocke, T. Osipov, H. Schmidt-Böcking, and R. Dörner, *Phys. Rev. Lett.* **92**, 163001 (2004).
- [26] M. Gisselbrecht, M. Lavollée, A. Huetz, P. Bolognesi, L. Avaldi, D. P. Seccombe, and T. J. Reddish, *Phys. Rev. Lett.* **96**, 153002 (2006).
- [27] M. P. Jones, T. M. Austiny, J. B. Williams, and A. L. Landers, *J. Phys. Conf. Ser.* **194**, 102038 (2009).
- [28] A. L. Landers, E. Wells, T. Osipov, K. D. Carnes, A. S. Alnaser, J. A. Tanis, J. H. McGuire, I. Ben-Itzhak, and C. L. Cocke, *Phys. Rev. A* **70**, 042702 (2004).
- [29] F. W. Byron and C. J. Joachain, *Phys. Rev.* **164**, 1 (1967).
- [30] F. W. Byron and C. J. Joachain, *Phys. Lett. A* **24**, 616 (1967).
- [31] R. J. Tweed, *J. Phys. B: At. Mol. Phys.* **6**, 259 (1973).
- [32] R. J. Tweed, *J. Phys. B: At. Mol. Phys.* **6**, 270 (1973).
- [33] T. Geyer, *J. Phys. B: At. Mol. Opt. Phys.* **37**, 1215 (2004).
- [34] L. Adoui, C. Caraby, A. Cassimi, D. Lelièvre, J. P. Grandin, and A. Dubois, *J. Phys. B* **32**, 631 (1999).
- [35] M. Takahashi, N. Watanabe, Y. Khajuria, Y. Udagawa, and J. H. D. Eland, *Phys. Rev. Lett.* **94**, 213202 (2005).
- [36] M. S. Pindzola, F. J. Robicieux, J. P. Colgan, M. C. Witthoef, and J. A. Ludlow, *Phys. Rev. A* **70**, 032705 (2004).
- [37] M. S. Pindzola, F. Robicieux, and J. Colgan, *Phys. Rev. A* **76**, 024704 (2007).
- [38] M. S. Pindzola, F. Robicieux, and J. Colgan, *J. Phys. B: At. Mol. Opt. Phys.* **39**, L127 (2006).
- [39] M. S. Pindzola, J. A. Ludlow, F. Robicieux, J. Colgan, and D. C. Griffin, *J. Phys. B: At. Mol. Opt. Phys.* **42**, 215204 (2009).
- [40] M. S. Pindzola, C. P. Ballance, F. Robicieux, and J. Colgan, *J. Phys. B: At. Mol. Opt. Phys.* **43**, 105204 (2010).
- [41] I. A. Ivanov and A. S. Kheifets, *Phys. Rev. A* **85**, 013406 (2012).
- [42] W. Vanroose, F. Martin, T. N. Rescigno, and C. W. McCurdy, *Phys. Rev. A* **70**, 050703 (2004).
- [43] C. Champion, D. Oubaziz, H. Aouchiche, Yu. V. Popov, and C. Dal Cappello, *Phys. Rev. A* **81**, 032704 (2010).
- [44] D. Oubaziz, H. Aouchiche, and C. Champion, *Phys. Rev. A* **83**, 012708 (2011).
- [45] C. Dal Cappello, C. Champion, I. Kada, and A. Mansouri, *Phys. Rev. A* **83**, 062716 (2011).
- [46] C. Champion and R. D. Rivarola, *Phys. Rev. A* **82**, 042704 (2010).
- [47] F. Tarentelli, A. Tarentelli, and A. Sgamellotti, *J. Chem. Phys.* **83**, 4683 (1985).
- [48] C. Champion, J. Hanssen, and P. -A. Hervieux, *Phys. Rev. A* **63**, 052720 (2001).
- [49] C. Champion, J. Hanssen, and P. -A. Hervieux, *J. Chem. Phys.* **121**, 9423 (2004).
- [50] C. Champion, C. Dal Cappello, S. Houamer, and A. Mansouri, *Phys. Rev. A* **73**, 012717 (2006).
- [51] C. Champion, O. Boudrioua, C. Dal Cappello, Y. Sato, and D. Ohsawa, *Phys. Rev. A* **75**, 032724 (2007).
- [52] R. Moccia, *J. Chem. Phys.* **40**, 2186 (1964).
- [53] H. Trygve, P. Jorgensen, and J. Olsen, in *Molecular Electronic-Structure Theory* (Wiley, New York, 2000).
- [54] P. Defrance, T. M. Kereselidze, I. L. Noselidze, and M. F. Tzulukidze, *J. Phys. B: At. Mol. Opt. Phys.* **34**, 4957 (2001).
- [55] E. Bahati, H. Cherkani-Hassani, P. Defrance, J. J. Jureta, T. Kereselidze, Z. Machavariani, and I. Noselidze, *J. Phys. B: At. Mol. Opt. Phys.* **38**, 1261 (2005).